INTERNATIONAL JOURNAL OF
NUMERICAL ANALYSIS AND MODELING
Volume 6, Number 3, Pages 440–454

A THREE-STAGE OPERATOR-SPLITTING/FINITE ELEMENT METHOD FOR THE NUMERICAL SIMULATION OF LIQUID CRYSTAL FLOW

ROLAND GLOWINSKI, PING LIN, AND XING-BIN PAN

Abstract. In this article, we investigate the application of an operator-splitting/finite element method to the numerical simulation of a liquid crystal flow. The operator-splitting is achieved through three stages, so that each stage is simpler and easier to deal with than the step of any un-split implicit scheme. The first stage deals with the system coupling a Stokes equation for velocity with an equation modeling the diffusion of the liquid crystal director field. The second stage deals with the convection of both the velocity and director field; a wave-like equation approach is used to treat this advection part and proves being quite efficient. Finally, the third stage deals with the nonlinear terms; a (quasi) closed form solution can be derived for this stage. Overall, with this type of splitting, the nonlinear terms in the liquid crystal model can be treated quite easily. The results of several numerical experiments show the good performances of the three-stage splitting method discussed in this article.

Key Words. liquid crystal, incompressible flow, finite element method, operator-splitting method.

1. Introduction

The last two decades have been witnessing a strong interest among physicists, engineers and mathematicians for the theory and numerical modeling of liquid crystal related phenomena, including the flow of such materials. Liquid crystals do not show a single transition from solid to liquid, but rather a cascade of transitions involving new phases. The classical Oseen-Frank theory suggests that the nematic phase of liquid crystals can be described by a director field $\mathbf{d}$, which minimizes the so-called Oseen-Frank energy. The mathematical analysis and computational results for some special cases of the Oseen-Frank model can be found in [1, 4, 5, 11, 20, 12, 2, 3, 9, 17]. In order to describe liquid crystal flows we need not only the orientation, as represented by the director field $\mathbf{d}$, but also the velocity field $\mathbf{u}$. Ericksen and Leslie were able to derive a hydrodynamic model for nematic liquid crystals: a nematic flow behaves like a regular liquid with molecules of similar size. However, such a liquid displays anisotropic properties due to the molecule alignment described by the local director field $\mathbf{d}$. In order to facilitate the mathematical understanding of the Ericksen-Leslie theory, F. H. Lin and Liu proposed in [13] to consider a simplified model retaining most of mathematical and physical significance of the original model, but simple enough to make possible a rigorous mathematical

Received by the editors October 30, 2008 and, in revised form, January 5, 2009.
2000 *Mathematics Subject Classification.* 65M60, 76A15.

discussion. The model reads as follows:

$$\mathbf{u}_t + (\mathbf{u}\cdot\nabla)\mathbf{u} - \nu\nabla\cdot D(\mathbf{u}) + \nabla p + \lambda\nabla\cdot\left((\nabla\mathbf{d})^T\nabla\mathbf{d}\right) = \mathbf{0} \text{ in } \Omega\times(0,T), \tag{1}$$

$$\nabla\cdot\mathbf{u} = 0 \text{ in } \Omega\times(0,T), \tag{2}$$

$$\mathbf{d}_t + (\mathbf{u}\cdot\nabla)\mathbf{d} - \gamma\left(\Delta\mathbf{d} - f(\mathbf{d})\right) = \mathbf{0} \text{ in } \Omega\times(0,T) \tag{3}$$

where in (1)-(3): (i) Ω ($\subset \mathbf{R}^d$) denotes the flow region and $(0,T)$ the time interval during which the flow is taking place. (ii) $\mathbf{u}$ represents the flow velocity and p the associated pressure. (iii) $\mathbf{d}$ represents the orientation of the liquid crystal molecules. (iv) $D(\mathbf{u}) = (1/2)\left(\nabla\mathbf{u} + (\nabla\mathbf{u})^T\right)$ and $(\nabla\mathbf{d})_{ij} = \frac{\partial d_i}{\partial x_j}$. (v) $f(\mathbf{d}) = (1/\epsilon^2)(|\mathbf{d}|^2 - 1)\mathbf{d}$. The vector-valued functions $\mathbf{u}$ and $\mathbf{d}$ (resp., the real valued function p) are defined over $\Omega\times(0,T)$ and take their values in $\mathbf{R}^d$ (resp., $\mathbf{R}$). For our computations we will consider only test problems with $d = 2$. Concerning $f(\cdot)$, it is a *penalty operator*, used to enforce (approximately) the condition $|\mathbf{d}| = 1$ (where $|\mathbf{d}|$ denotes the canonical Euclidian norm of $\mathbf{d}$; actually, $f(\mathbf{d})$ is the differential at $\mathbf{d}$ of the *penalty functional* F defined by

$$F(\mathbf{d}) = (1/4\epsilon^2)(|\mathbf{d}|^2 - 1)^2.$$

The condition $|\mathbf{d}| = 1$ follows from the fact that the liquid crystal molecules are of similar size. Equation (1) describes the conservation of the linear momentum; it combines terms describing the flow of an isotropic fluid with an additional nonlinear term which is anisotropic. The second equation models the incompressibility of the liquid crystal material. The third equation is associated with the conservation of the angular momentum.

Of course, (1)-(3) have to be completed by initial and boundary conditions, such as:

$$\mathbf{u}|_{t=0} = \mathbf{u}_0, \quad \mathbf{d}|_{t=0} = \mathbf{d}_0, \quad \mathbf{u}|_{\partial\Omega} = \mathbf{u}_0|_{\partial\Omega} = \mathbf{g}_\mathbf{u}, \quad \mathbf{d}|_{\partial\Omega} = \mathbf{g}_\mathbf{d}. \tag{4}$$

Even if the initial velocity is zero, the evolution of the director field may induce a velocity, which in turn will affect the evolution of the director field. Since the mathematical study of these interactions (between $\mathbf{u}$ and $\mathbf{d}$) is difficult, their numerical study is a most natural alternative. In [18] (resp., [19]), Liu & Walkington used an energy preserving C^1-conforming finite element method (resp., mixed finite element method) for the solution of problem (1)-(4). In [16], Lin & Liu further simplified the space approximations discussed in [18, 19] by deriving an energy preserving C^0-conforming finite element method. Some other methods have been used for the space approximation of (1)-(4); for example, the spectral method discussed in [6] appear to be efficient on rectangular domains when $\mathbf{u}$ and $\mathbf{d}$ verify periodic boundary conditions.

Considering the good results presented in [9], by the authors of the present article, for a simplified Oseen-Frank liquid crystal model, we would like to apply to the solution of problem (1)-(4) a variation of the operator-splitting scheme we employed in the above reference. As shown in, e.g., [8], the operator-splitting methodology provides quite often simple and efficient methods for the solution of complicated partial differential equations. In the particular case of problems such as (1)-(4), an appropriate operator-splitting time discretization scheme will allow us to treat rather easily the contribution of the nonlinear operator $f(\cdot)$, through the solution of simple cubic equations in one variable, reducing thus considerably the associated computational time compared to an implicit un-split time discretization scheme. In this article we are going to discuss a three-stage time-splitting scheme for the solution of problem (1)-(4); this scheme will have the 'nice' properties mentioned

above concerning the treatment of the nonlinear operator $f(\cdot)$. Our method is easy to implement, and due to its modularity, it can take advantage of existing solvers and mesh generators, further reducing thus the complexity of the computer implementation.

A weak formulation and a fully discrete scheme combining finite element approximation with the backward Euler time-discretization scheme will be provided in Section 2. The three-stage operator-splitting time discretization scheme will be described in Section 3. In Section 4, we will use the methodology discussed in the Sections 2 and 3, in order to solve test problems of physical interest associated with various shapes for Ω.

We hope that the numerical results presented in this article will motivate analysts at further investigating the mathematical properties of the solution of liquid crystal flow problems.

2. Weak formulation and full discretization of problem (1)-(4)

From now on, we assume that Ω is bounded in $\mathbf{R}^d$ with $d = 2$ or 3. We denote by Γ the boundary $\partial\Omega$ of Ω and we assume that Γ is reasonably smooth (Lipschitz-continuous, for example). Define the functional spaces $\mathbf{H}^1(\Omega)$, $\mathbf{H}^1_{\mathbf{g}}$ and $\mathbf{L}^2(X)$ by $\mathbf{H}^1(\Omega) = (H^1(\Omega))^d$, $\mathbf{H}^1_{\mathbf{g}} = \{\mathbf{v}|\mathbf{v} \in \mathbf{H}^1(\Omega), \mathbf{v} = \mathbf{g} \text{ on } \Gamma\}$ and $\mathbf{L}^2(X) = (L^2(X))^d$, respectively. A *weak formulation* of problem (1)-(4) reads as follows:

Find $\{\mathbf{u}, p, \mathbf{d}\} \in [\mathbf{H}^1(0,T;\mathbf{H}^{-1}(\Omega)) \cap \mathbf{L}^2(0,T;\mathbf{H}^1(\Omega))] \times L^2(0,T;L^2(\Omega)/\mathbf{R}) \times [\mathbf{H}^1(0,T;\mathbf{H}^1(\Omega)) \cap \mathbf{L}^2(0,T;\mathbf{H}^1(\Omega))]$ *such that a.e. on* $(0,T)$:

$$\int_\Omega \left(\mathbf{u}_t \cdot \mathbf{v} + (\mathbf{u}\cdot\nabla)\mathbf{u}\cdot\mathbf{v} + \nu\nabla\mathbf{u} : \nabla\mathbf{v} d\mathbf{x} - p(\nabla\cdot\mathbf{v}) - \lambda(\nabla\mathbf{d})^T\nabla\mathbf{d} : \nabla\mathbf{v}\right) d\mathbf{x} = \mathbf{0}$$

$$\forall \mathbf{v} \in \mathbf{H}^1_0(\Omega), \tag{5}$$

$$\int_\Omega (\nabla\cdot\mathbf{u}) q d\mathbf{x} = 0 \quad \forall q \in L^2(\Omega), \tag{6}$$

$$\int_\Omega \left(\mathbf{d}_t \cdot \mathbf{e} + (\mathbf{u}\cdot\nabla)\mathbf{d}\cdot\mathbf{e} + \gamma(\nabla\mathbf{d} : \nabla\mathbf{e} - f(\mathbf{d})\cdot\mathbf{e})\right) d\mathbf{x} = \mathbf{0} \quad \forall \mathbf{e} \in \mathbf{H}^1_0(\Omega). \tag{7}$$

$$\mathbf{u}|_{t=0} = \mathbf{u}_0, \quad \mathbf{d}|_{t=0} = \mathbf{d}_0, \quad \mathbf{u}|_\Gamma = \mathbf{g}_\mathbf{u}, \quad \mathbf{d}|_\Gamma = \mathbf{g}_\mathbf{d}. \tag{8}$$

Rigorously speaking, the functional space we need is $\mathbf{W}^{1,3}(\Omega)$ for $\mathbf{d}$ and the test function of the momentum equation. But we will not explore this in this computational paper. We are going to use C^0 finite elements in our computation, which are conformal to all these functional spaces. Problem (5)-(8) is equivalent to (1)-(4); it can be solved by a method combining finite differences for the time-discretization with finite elements for the space approximation. A fully implicit time-discretization scheme will guarantee temporal stability (even so, the time-discretization step has to be small enough, since, in particular, the nonlinear operator $f(\cdot)$ is not monotone). Concerning the space approximation of problem (5)-(8), let us denote by $\mathbf{H}$ the space $\mathbf{H}^1(\Omega) \times L^2(\Omega) \times \mathbf{H}^1(\Omega)$ and by $\mathbf{H}_0$ the space $\mathbf{H}^1_0(\Omega) \times L^2(\Omega)/\mathbf{R} \times \mathbf{H}^1_0(\Omega)$; we approximate $\mathbf{H}$ and $\mathbf{H}_0$ by

$$\mathbf{H}_h = \mathbf{V}_h \times Q_h \times \mathbf{E}_h (\subset \mathbf{H}) \tag{9}$$

and

$$\mathbf{H}_{0h} = \mathbf{V}_{0h} \times Q_h/\mathbf{R} \times \mathbf{E}_{0h} (\subset \mathbf{H}_0), \tag{10}$$

respectively, where, in (9), (10), $\mathbf{V}_h$, Q_h and $\mathbf{E}_h$ are finite element spaces associated with a triangulation T_h of Ω , and where $\mathbf{V}_{0h}$ and $\mathbf{E}_{0h}$ are defined by

$$\mathbf{V}_{0h} = \{\mathbf{v}|\mathbf{v} \in \mathbf{V}_h,\ \mathbf{v} = \mathbf{0} \text{ on } \Gamma\} \text{ and } \mathbf{E}_{0h} = \{\mathbf{e}|\mathbf{e} \in \mathbf{E}_h,\ \mathbf{e} = \mathbf{0} \text{ on } \Gamma\}.$$

Taking $\mathbf{E}_h = \mathbf{V}_h$ and therefore $\mathbf{E}_{0h} = \mathbf{V}_{0h}$ is a sensible choice. With Δt (> 0) a *time-discretization step* (that we suppose constant for simplicity), a backward Euler based *fully discrete scheme* for the space-time approximation of problem (5)-(8) reads as follows:

(11) An approximation $\{\mathbf{u}_h^0, \mathbf{d}_h^0\}$ of $\{\mathbf{u}_0, \mathbf{d}_0\}$ is given in $\mathbf{V}_h \times \mathbf{E}_h$.

For $n > 0$, being known, we obtain $\{\mathbf{u}_h^n, p_h^n, \mathbf{d}_h^n\}$ from the solution in $\mathbf{H}_h$ of the following discrete elliptic variational system:

$$\int_\Omega \left[\frac{\mathbf{u}_h^n - \mathbf{u}_h^{n-1}}{\Delta t} \cdot \mathbf{v} + (\mathbf{u}_h^n \cdot \nabla)\mathbf{u}_h^n \cdot \mathbf{v} + \nu \nabla \mathbf{u}_h^n : \nabla \mathbf{v} - p_h^n (\nabla \cdot \mathbf{v}) \right.$$
$$\left. - \lambda (\nabla \mathbf{d}_h^n)^T \nabla \mathbf{d}_h^n : \nabla \mathbf{v} \right] d\mathbf{x} = \mathbf{0},\ \forall \mathbf{v} \in \mathbf{V}_{0h}, \tag{12}$$

$$\int_\Omega (\nabla \cdot \mathbf{u}_h^n)\ q\ d\mathbf{x} = 0,\ \forall q \in Q_h, \tag{13}$$

$$\int_\Omega \left[\frac{\mathbf{d}_h^n - \mathbf{d}_h^{n-1}}{\Delta t} \cdot \mathbf{e} + (\mathbf{u}_h^n \cdot \nabla)\mathbf{d}_h^n \cdot \mathbf{e} + \gamma [\nabla \mathbf{d}_h^n : \nabla \mathbf{e} - f(\mathbf{d}_h^n) \cdot \mathbf{e}] \right] d\mathbf{x} = 0, \tag{14}$$
$$\forall \mathbf{e} \in \mathbf{E}_{0h},$$

$$\mathbf{u}_h^n|_\Gamma = \mathbf{g}_{\mathbf{u}h},\ \mathbf{d}_h^n|_\Gamma = \mathbf{g}_{\mathbf{d}h}, \tag{15}$$

where, in (15), $\mathbf{g}_{\mathbf{u}h}$ and $\mathbf{g}_{\mathbf{d}h}$ are approximations of $\mathbf{g}_\mathbf{u}$ and $\mathbf{g}_\mathbf{d}$ belonging to the spaces $\gamma_0 \mathbf{V}_h$ and $\gamma_0 \mathbf{E}_h$ with γ_0 the *trace operator* from $\mathbf{H}^1(\Omega)$ onto $\mathbf{H}^{\frac{1}{2}}(\Gamma)$ defined by $\gamma_0 \mathbf{v} = \mathbf{v}|_\Gamma$.

The finite-dimensional problem (12)-(15) is highly nonlinear with a strong coupling between (12), (13) and (14). A simple way to make the above system less nonlinear and weaken the coupling between its various equations is to linearize the advection terms in (12) and (14); this is easily achieved by substituting $(\mathbf{u}_h^{n-1} \cdot \nabla)\mathbf{u}_h^n$ (resp., $(\mathbf{u}_h^{n-1} \cdot \nabla)\mathbf{d}_h^n$) to $(\mathbf{u}_h^n \cdot \nabla)\mathbf{u}_h^n$ (resp., $(\mathbf{u}_h^n \cdot \nabla)\mathbf{d}_h^n$) in (12) (resp., (14)); based on our long experience with incompressible viscous flows, we can anticipate that the resulting scheme will be almost as stable than scheme (12)-(15), its main drawback being that the associated stiffness matrices vary with n and that the analogue of (14) is still highly nonlinear. A simple way to overcome these difficulties is to apply to the solution of problem (5)-(8) a well-chosen *operator-splitting* method, following thus a strategy which has been quite successful for the numerical solution of simpler liquid-crystal problems (see [10, 9] for details).

3. A three-stage operator splitting for the solution of problem (1)-(4)

In order to simplify the presentation, we will describe our operator-splitting method when applied to the continuous problem (1)-(4); its finite element implementation is straightforward. Our three-stage splitting scheme reads as follows (with $t^n = n\Delta t$):

Initialization:

$$\{\mathbf{u}^0, \mathbf{d}^0\} = \{\mathbf{u}_0, \mathbf{d}_0\}. \tag{16}$$

For $n \geq 0$, we obtain $\{\mathbf{u}^{n+1}, p^{n+1}, \mathbf{d}^{n+1}\}$ from $\{\mathbf{u}^n, \mathbf{d}^n\}$ via the solution of

Step 1: *Diffusion sub-problems*

$$\frac{\mathbf{u}^{n+\frac{1}{3}}-\mathbf{u}^n}{\Delta t}-\mu\nabla^2\mathbf{u}^{n+\frac{1}{3}}+\nabla p^{n+1}=\mathbf{0} \text{ in } \Omega, \tag{17}$$

$$\nabla\cdot\mathbf{u}^{n+\frac{1}{3}}=0 \text{ in } \Omega, \tag{18}$$

$$\frac{\mathbf{d}^{n+\frac{1}{3}}-\mathbf{d}^n}{\Delta t}-\gamma\nabla^2\mathbf{d}^{n+\frac{1}{3}}=\mathbf{0} \text{ in } \Omega, \tag{19}$$

$$\mathbf{u}^{n+\frac{1}{3}}=\mathbf{g_u} \text{ on } \Gamma,\ \mathbf{d}^{n+\frac{1}{3}}=\mathbf{g_d} \text{ on } \Gamma. \tag{20}$$

Step 2: *Advection sub-problems*

$$\frac{\partial\mathbf{u}}{\partial t}+(\mathbf{u}^{n+\frac{1}{3}}\cdot\nabla)\mathbf{u}=\mathbf{0} \text{ in } \Omega\times(t^n,t^{n+1}) \tag{21}$$

$$\frac{\partial\mathbf{d}}{\partial t}+(\mathbf{u}^{n+\frac{1}{3}}\cdot\nabla)\mathbf{d}=\mathbf{0} \text{ in } \Omega\times(t^n,t^{n+1}), \tag{22}$$

$$\mathbf{u}(t^n)=\mathbf{u}^{n+\frac{1}{3}},\ \mathbf{d}(t^n)=\mathbf{d}^{n+\frac{1}{3}}, \tag{23}$$

$$\{\mathbf{u},\mathbf{d}\}=\{\mathbf{g_u},\mathbf{g_d}\} \text{ on } \Gamma_-\times(t^n,t^{n+1}), \tag{24}$$

$$\mathbf{u}^{n+\frac{2}{3}}=\mathbf{u}(t^{n+1}),\ \mathbf{d}^{n+\frac{2}{3}}=\mathbf{d}(t^{n+1}) \tag{25}$$

with $\Gamma_-=\{\mathbf{x}\mid\mathbf{x}\in\Gamma,\mathbf{g_u}(\mathbf{x})\cdot\mathbf{n}(\mathbf{x})<0\}$, $\mathbf{n}$ *being the outward unit vector normal at* Γ.

Step 3: *Nonlinear sub-problems:*

$$\frac{\mathbf{d}^{n+1}-\mathbf{d}^{n+\frac{2}{3}}}{\Delta t}+\gamma f(\mathbf{d}^{n+1})=\mathbf{0} \tag{26}$$

$$\frac{\mathbf{u}^{n+1}-\mathbf{u}^{n+\frac{2}{3}}}{\Delta t}=-\lambda\nabla\cdot((\nabla\mathbf{d}^{n+1})^T\nabla\mathbf{d}^{n+1}) \text{ in } \Omega. \tag{27}$$

Through the above three-stage operator-splitting scheme, we observe that there is no coupled system to solve to obtain at each time step the values of $\mathbf{u}$ and $\mathbf{d}$. Moreover, in Step 1, the stiffness matrix for either $\mathbf{u}$ or $\mathbf{d}$ is *independent* of the time step n since we do not modify Δt; if one chooses a *direct method* (Gauss' or Cholesky's, for example) for the solution of the associated linear systems, these stiffness matrices need to be factored only once; this reduces considerably the computational time. In Step 3, the nonlinear equation providing $\mathbf{d}^{n+1}$ can be solved *point-wise* (in practice at the grid-points of a finite difference or a finite element mesh); a.e. on Ω , we have to solve the following *cubic equation* in $\mathbf{R}^d$:

$$\mathbf{d}^{n+1}(\mathbf{x})+\alpha(|\mathbf{d}^{n+1}(\mathbf{x})|^2-1)\mathbf{d}^{n+1}(\mathbf{x})=\mathbf{d}^{n+\frac{2}{3}}(\mathbf{x}), \tag{28}$$

where, in (28), $\alpha=\gamma\Delta t/\epsilon^2$. If $\alpha\leq 1$ equation (28) has a unique solution, given by

$$\mathbf{d}^{n+1}(\mathbf{x})=\frac{\mathbf{d}^{n+\frac{2}{3}}(\mathbf{x})}{1-\alpha+\alpha|\mathbf{d}^{n+1}(\mathbf{x})|^2}, \tag{29}$$

where, in (29), $|\mathbf{d}^{n+1}(\mathbf{x})|$ satisfies the following cubic equation:

$$\alpha z^3+(1-\alpha)z-|\mathbf{d}^{n+\frac{2}{3}}(\mathbf{x})|=0. \tag{30}$$

If $\alpha<1$, in order to compute the unique solution of equation (30), we advocate the Newton's method initialized by $|\mathbf{d}^{n+\frac{2}{3}}|$. If $\alpha=1$ one has

$$\mathbf{d}^{n+1}(\mathbf{x})=\frac{\mathbf{d}^{n+\frac{2}{3}}(\mathbf{x})}{|\mathbf{d}^{n+\frac{2}{3}}(\mathbf{x})|^{2/3}} \quad \text{if } \mathbf{d}^{n+\frac{2}{3}}(\mathbf{x})\neq\mathbf{0}. \tag{31}$$

If $\alpha > 1$, relations (28) and (29) still apply; in that case we suggest to take for $|\mathbf{d}^{n+1}(\mathbf{x})|$ the unique positive solution of (29) (to compute it we can use the Newton's method initialized by $z = 1$).
Concerning Step 2, we will take the approach already used in [7] for the simulation of a variety of Newtonian and non-Newtonian incompressible viscous flows (possibly temperature dependent). It relies on a *wave-like* reformulation of the advection problems and can be described as follows:

Consider the following pure advection problem

$$\frac{\partial \phi}{\partial t} + \mathbf{V} \cdot \nabla \phi = 0 \quad \text{in } \Omega \times (t_0, t_f) \tag{32}$$

$$\phi(t_0) = \phi_0, \tag{33}$$

$$\phi = g \quad \text{on } \Gamma_- \times (t_0, t_f), \tag{34}$$

where: (i) $\Gamma_- = \{\mathbf{x} \mid \mathbf{x} \in \Gamma, \mathbf{V}(\mathbf{x}) \cdot \mathbf{n}(\mathbf{x}) < 0\}$. (ii) $\nabla \cdot \mathbf{V} = 0$ *and* $\frac{\partial \mathbf{V}}{\partial t} = \mathbf{0}$. (iii) $\frac{\partial g}{\partial t} = 0$.

As shown in, e.g., [7] proving the uniqueness of a solution to problem (32-(34) is an easy matter (unlike proving the existence of solutions, an issue we will not address here). Differentiating (32) with respect to t, we observe that (32)-(34) implies (formally, at least) that ϕ verifies also

$$\frac{\partial^2 \phi}{\partial t^2} - \nabla \cdot ((\mathbf{V} \cdot \nabla \phi)\mathbf{V}) = 0, \quad \text{in } \Omega \times (t_0, t_f), \tag{35}$$

$$\phi(t_0) = \phi_0, \quad \frac{\partial \phi}{\partial t}(t_0) = -\mathbf{V} \cdot \nabla \phi_0, \tag{36}$$

$$\phi = g \text{ on } \Gamma_- \times (t_0, t_f), \ \mathbf{V} \cdot \mathbf{n}(\frac{\partial \phi}{\partial t} + \mathbf{V} \cdot \nabla \phi) = 0 \text{ on } (\Gamma \backslash \Gamma_-) \times (t_0, t_f). \tag{37}$$

One can easily prove that the wave-like problem (35)-(37) has a unique solution, this solution is necessarily unique (see, e.g., [7] for details). In order to solve the above wave-problem by a method combining finite differences for the time-discretization and finite element for the space approximation we can take advantage of the following *equivalent weak formulation* of problem (35)-(37), for a.e. $t \in (t_0, t_f)$:

$$\int_\Omega \left[\frac{\partial^2 \phi}{\partial t^2} \psi + (\mathbf{V} \cdot \nabla \phi)(\mathbf{V} \cdot \nabla \psi) \right] d\mathbf{x} + \int_{\Gamma \backslash \Gamma_-} \mathbf{V} \cdot \mathbf{n} \frac{\partial \phi}{\partial t} \psi d\Gamma = 0, \ \forall \psi \in V_-, \tag{38}$$

$$\phi(t_0) = \phi_0, \ \frac{\partial \phi}{\partial t}(t_0) = -\mathbf{V} \cdot \nabla \phi_0, \tag{39}$$

$$\phi = g \text{ on } \Gamma_-, \tag{40}$$

with $V_- = \{\psi \mid \psi \in H^1(\Omega), \ \psi|_{\Gamma_-} = 0\}$. Concerning the *time-discretization* of (38)-40) we follow [7], that is:

(i) Let $\tau = \frac{t_f - t_0}{Q}$, Q being a positive integer ($Q = 5$, typically).
(ii) Take

$$\phi^0 = \phi_0. \tag{41}$$

(iii) Compute ϕ^1 and ϕ^{-1}, verifying $\phi^1 = g$ on Γ_- and $\phi^{-1} = g$ on Γ_-, from

$$\int_\Omega \frac{\phi^1 - \phi^{-1}}{2\tau}\psi \, d\mathbf{x} = -\int_\Omega \mathbf{V}\cdot\nabla\phi_0\psi \, d\mathbf{x}, \ \forall\psi \in V_-, \tag{42}$$

$$\int_\Omega \left[\frac{\phi^1 - 2\phi^0 + \phi^{-1}}{\tau^2}\psi + (\mathbf{V}\cdot\nabla\phi^0)(\mathbf{V}\cdot\nabla\psi)\right] d\mathbf{x} + \int_{\Gamma\setminus\Gamma_-} \mathbf{V}\cdot\mathbf{n}\frac{\phi^1 - \phi^{-1}}{2\tau}\psi \, d\Gamma = 0, \ \forall\psi \in V_-. \tag{43}$$

(iv) For $q = 1, \ldots, Q-1$, ϕ^q and ϕ^{q-1} being known, compute ϕ^{q+1} verifying $\phi^{q+1} = g$ on Γ_-, from

$$\int_\Omega \left[\frac{\phi^{q+1} - 2\phi^q + \phi^{q-1}}{\tau^2}\psi + (\mathbf{V}\cdot\nabla\phi^q)(\mathbf{V}\cdot\nabla\psi)\right] d\mathbf{x} + \int_{\Gamma\setminus\Gamma_-} \mathbf{V}\cdot\mathbf{n}\frac{\phi^{q+1} - \phi^{q-1}}{2\tau}\psi d\Gamma = 0, \ \forall\psi \in V_-. \tag{44}$$

The finite element implementation of the scheme (42)-(44) is straightforward (it has been discussed with many details in [7]).

Remark 3.1. *In this article, the* divergence free condition *(18) is treated by a so-called* sequential regularization *formulation, so that general C^0 polynomial elements can be used and that we do not need to worry beforehand whether our finite element approximation of Stokes problem (17),(18),(20) passes the Babuska-Brezzi test (although this test may be automatically satisfied for formulations like those discussed in, e.g.,* [14, 15]*). For this flow problem discussed in this article, it turns out that the* penalty *formulation, which is the simplest sequential regularization formulation, works very well. Thus, in practice, we replace (18) by*

$$\int_\Omega (\nabla\cdot\mathbf{u}_h^{n+\frac{1}{3}} + \delta \, p_h^{n+1}) \, q \, d\mathbf{x} = 0, \ \forall q \in Q_h. \tag{45}$$

We choose $\delta = 10^{-6}$ for our computation.

4. Numerical experiments

In this section, we will apply a finite element realization of the three-stage splitting method discussed in Section 3, to the solution of two-dimensional liquid crystal flow test problems. The first test problem originates from [18, 19, 13] where one discusses its un-split solution using C^1-conforming, C^0 mixed and C^0-conforming finite element approximations. As in the above references, we take $\lambda = \nu = \gamma = 1$ and $\Omega = (-1, 1)^2$ and use a uniform finite element triangulation (like the one in Figure 1) for the space approximation. We use C^0-conforming piecewise quadratic finite element space approximations for $\mathbf{u}$ and $\mathbf{d}$, while C^0-conforming piecewise linear approximations are used for p. The resulting approximation of the Stokes problems in (17), (18), (20) is therefore of the Hood-Taylor type (see, e.g., [7][Chapter 5] for further information on the Hood-Taylor approximation of Stokes problems), implying that Babuska-Brezzi inf-sup condition is automatically verified and that the penalty approximation associated with (45) is not a necessity anymore. We kept nevertheless (45) has an extra robustness device, making possible the solution of the associated discrete Stokes problem by a direct method (the iterative solution of continuous and discrete Stokes problem is discussed in [7][Chapters 4 and 5]).

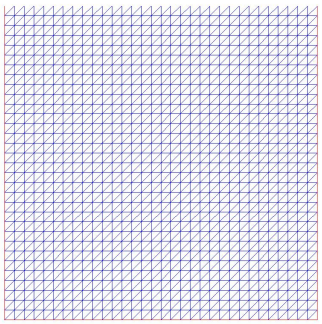

FIGURE 1. A uniform triangulation on a 32×32 grid

Example 4.1. *We consider an example borrowed from* [18]. *The initial director field* $\mathbf{d}^0$ *is given by*

$$\mathbf{d}^0(\mathbf{x}) = \tilde{\mathbf{d}}(\mathbf{x})/\sqrt{|\tilde{\mathbf{d}}(\mathbf{x})|^2 + \eta^2},$$

where

$$\tilde{\mathbf{d}}(\mathbf{x}) = (x_1^2 + x_2^2 - \alpha^2, 2\alpha x_2)$$

and $\alpha = 0.5$. *This director field has singularities at* $\mathbf{x} = (\pm\alpha, 0)$ *with unit degrees of opposite signs. We choose this example in order to illustrate how director field singularities of opposite sign in the director field will move together and annihilate each other. Concerning the initial velocity, we took* $\mathbf{u}^0 = \mathbf{0}$, *first. For boundary conditions we took*

$$\mathbf{g}_\mathbf{u} = \mathbf{u}^0|_\Gamma, \ \mathbf{g}_\mathbf{d} = \mathbf{d}^0|_\Gamma. \tag{46}$$

For these computations, we took $\epsilon^2 = \eta^2 = 2.5 \times 10^{-3}$ *and* $\Delta t = 10^{-4}$. *On Figure 2 we have represented the initial director field (left) and the computed director field at* $t = 1$ *(right), the computations taking place on a* 32×32 *finite element grid. Figure 3 shows the computed director (left) and velocity (right) fields near the time of annihilation of singularities. In our computations the energy is decreasing and* $|\mathbf{d}| \leq 1$, *which shows that our method well preserves the energy law and the maximum principle for the director variable* $\mathbf{d}$. *Also, the singularity transport pattern is the same as those in* [18, 13] *for the same example.*

Next, we did a simulation with $\mathbf{d}^0$ *and* $\mathbf{g}_\mathbf{d}$ *as before, but this time we choose for initial velocity* $\mathbf{u}^0$ *the rotating field* $(-\omega x_2, \omega x_1)$, *with* $\omega = 20$ *(approximately three revolutions per time unit) and* $\mathbf{g}_\mathbf{u}$ *still defined from* $\mathbf{u}^0$ *by (46). Figure 4 depicts the velocity field at* $t = \Delta t$ *(left) and the computed velocity field at* $t = 0.5$ *(near steady state); we observe that the velocity field almost did not change through the time. Figure 5 depicts the director field at (a)* $t = 0.1$, *(b)* $t = 0.2$, *(c)* $t = 0.24$ *(annihilation) and (d)* $t = 0.5$ *(near steady state). The computed results coincide essentially with those in* [18, 13].

Example 4.2. *In this example, we consider a domain* Ω *with a circular hole in the center of a square, as shown in Figure 6, where a triangulation of* Ω *is also depicted. The initial director field is defined as in Example 4.1, as is* $\mathbf{g}_\mathbf{d}$. *To solve the corresponding liquid crystal flow problem we employ the operator-splitting/finite*

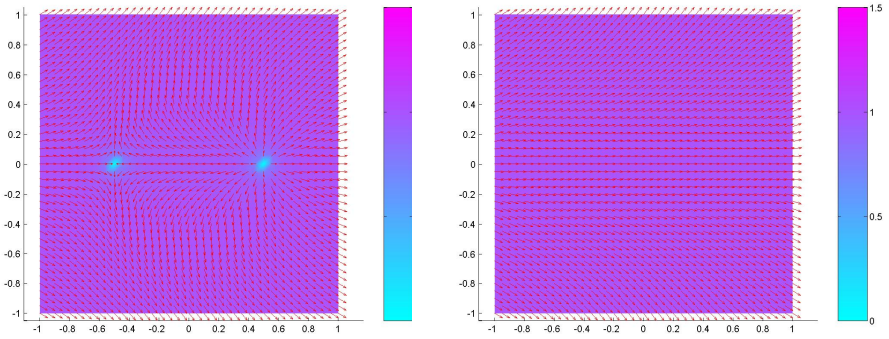

FIGURE 2. Example 4.1 ($\mathbf{u}^0 = \mathbf{0}$): Initial director field (left), director field at $t = 1$ (right, very close to the steady state)

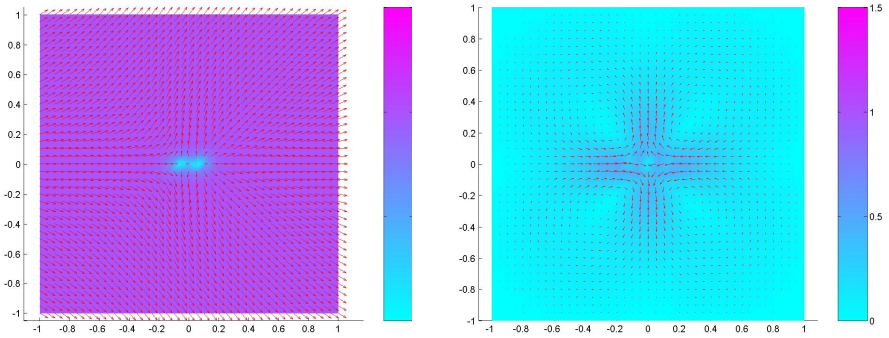

FIGURE 3. Example 4.1 ($\mathbf{u}^0 = \mathbf{0}$): Director (left) and velocity (right) fields near the annihilation time

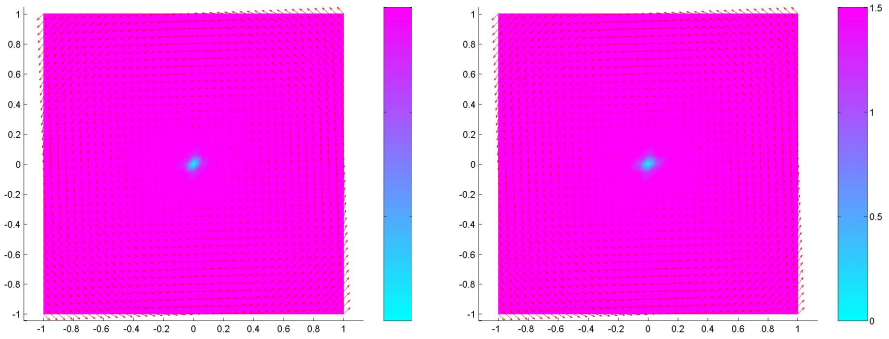

FIGURE 4. Example 4.1 ($\mathbf{u}^0(\mathbf{x}) = (-\omega x_2, \omega x_1)$): Rotational velocity field

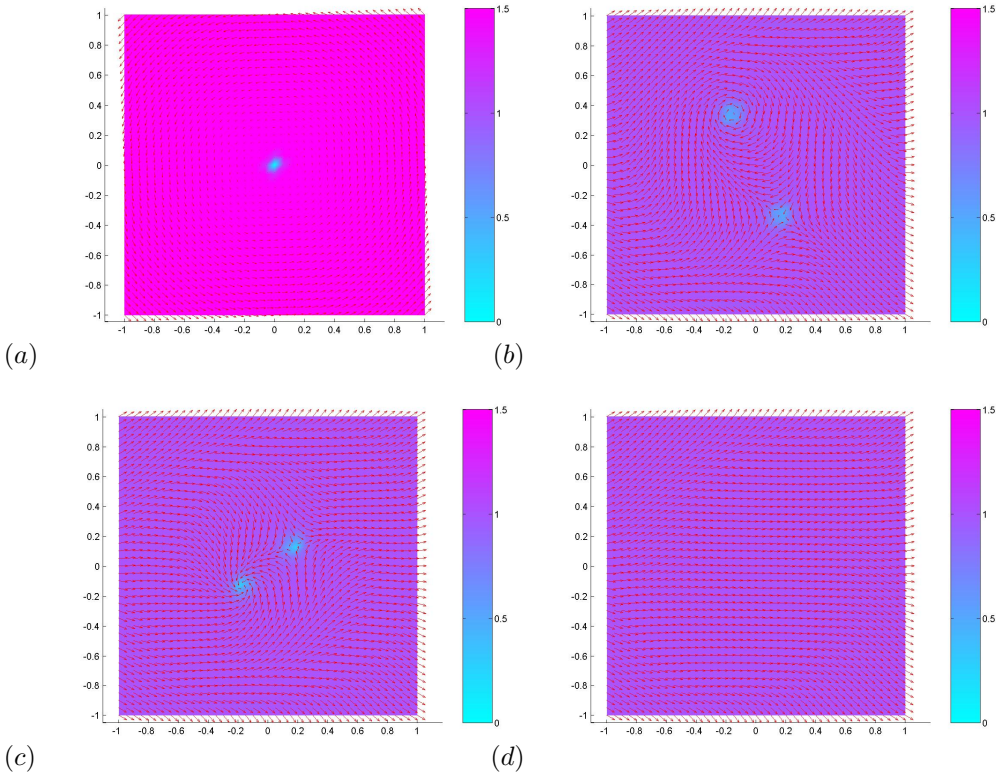

FIGURE 5. Example 4.1 ($\mathbf{u}^0(\mathbf{x}) = (-\omega x_2, \omega x_1)$): Director field at (a) $t = 0.1$, (b) $t = 0.2$, (c) $t = 0.24$ (annihilation) and (d) $t = 0.5$ (steady state)

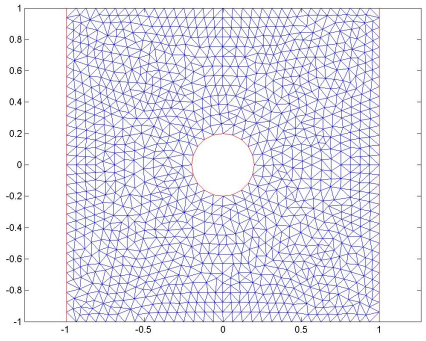

FIGURE 6. A triangular mesh on a square domain with a circular hole

element based methodology we used to treat Example 4.1, the finite element triangulation being the one depicted in Figure 6 (it contains 2254 triangles); the other physical and computational parameters are as in the above example.

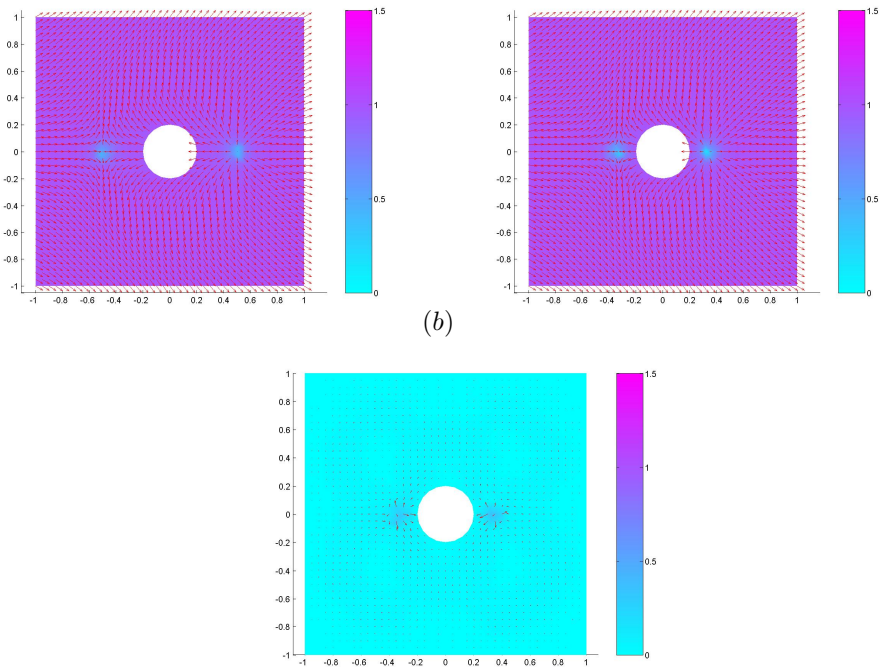

FIGURE 7. Example 4.2 ($\mathbf{u}^0 = \mathbf{0}$): (a) Initial director field. (b) Director field at $t = 0.3$. (c) Velocity field at $t = 0.3$

Assuming that $\mathbf{u}^0 = \mathbf{0}$ *and* $\mathbf{g_u} = \mathbf{0}$, *we obtain the results depicted in Figures 7. We observe that the singular points move towards the center of* Ω; *however, they eventually stop near the boundary of the circular hole. If* $\mathbf{u}^0 = (-\omega x_2, \omega x_1)$, *with* $\mathbf{g_u}$ *still given by (46), we obtain the results depicted in Figure 8; they show that the two singularities rotate around the circular hole and suggest that it is unlikely that they will meet and annihilate each other.*

Example 4.3. *We consider finally an example where the initial director field is defined by*

$$\mathbf{d}^0(\mathbf{x}) = -(cos2\theta, sin2\theta),$$

with $\cos\theta = x_1/r$, $\sin\theta = x_2/r$ *and* $r = \sqrt{x_1^2 + x_2^2}$. *The domain* Ω *is the square encountered in Example 4.1. The boundary function* $\mathbf{g_d}$ *is still defined from* $\mathbf{d}^0$ *by relation (46). Concerning the initial velocity field, we take for* $\mathbf{u}^0$ *the steady state solution of the celebrated wall-driven cavity flow problem with* $\mathbf{u} = (1, 0)$ *on the top boundary and* $\mathbf{u} = \mathbf{0}$ *elsewhere. For boundary conditions on* $\mathbf{u}$ *and* $\mathbf{d}$ *in the liquid crystal flow problem, we still use (46) to define* $\mathbf{g_u}$ *and* $\mathbf{g_d}$ *from* $\mathbf{u}^0$ *and* $\mathbf{d}^0$, *respectively. All the other physical and computational parameters are as in Example 4.1. The solution of a simplified Oseen-Frank minimum energy model with the same initial director field was computed in* [9] *and two singularity segments were observed in the steady state solution. From the theory of harmonic maps with the same kind of topological degree 2 boundary condition, one expects a steady state solution with two singularities at least if the domain* Ω *has a smooth boundary. For this liquid crystal cavity flow problem we observe on Figures 9 to 11 that two singularities*

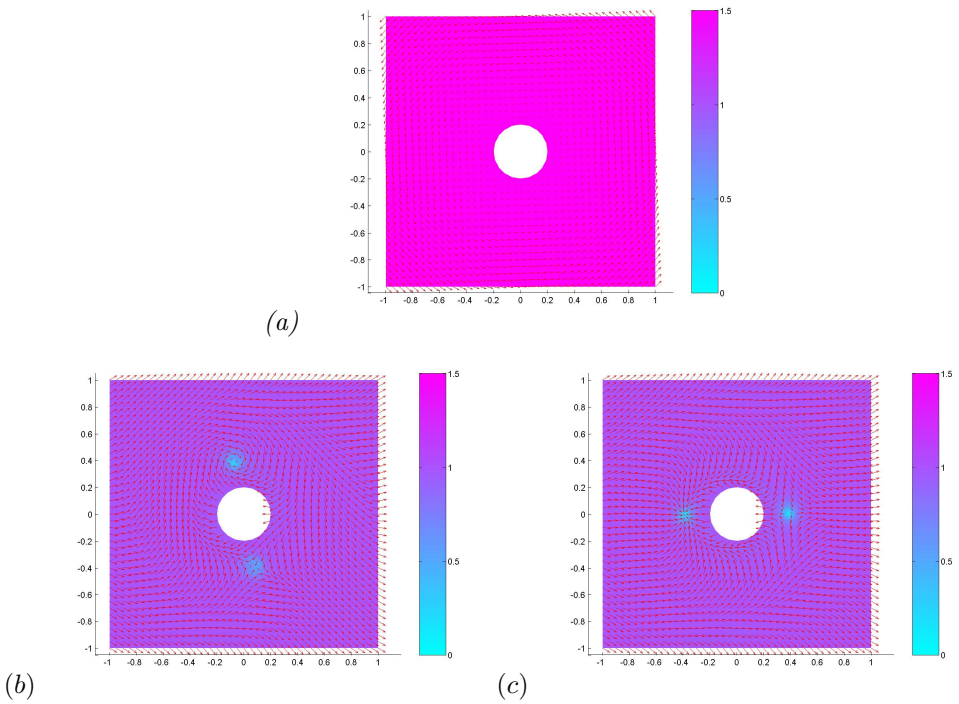

FIGURE 8. Example 4.2 ($\mathbf{u}^0(\mathbf{x}) = (-\omega x_2, \omega x_1)$): (a) Initial velocity field. (b) Director field at $t = 0.1$. (c) Director field at $t = 0.2$

separate from the initial singularity at the center of Ω*, then move apart, roughly along a diagonal of the square domain, and then slowly shuffle off the diagonal line until being close to the steady state before* $t = 20$ *(we computed the solution till* $t = 60$ *and did not observe any significant difference from the solution at* $t = 20$*).*

Acknowledgments

The work of Lin were partially supported by Singapore Academic Research Grants no. R-146-000-064-112 and no. R-146-000-099-112. The work of Pan was partially supported by the National Natural Science Foundation of China, the Science Foundation of the Ministry of Education of China grant no. 20060269012, and the National Basic Research Program of China grant no. 2006CB805902.

References

[1] P. Aviles and Y. Giga, A mathematical problem related to the physical theory of liquid crystal configurations, Proc. Centre Math. Anal. Austral. Nat. Univ., **12** (1987), 1-16.

[2] R. Cohen, S.-Y. Lin and M. Luskin, Relaxation and gradient methods for molecular orientation in liquid crystals, Comput. Physics Comm., **53** (1989), 455-465.

[3] R. Cohen, R. Hardt, D. Kinderlehrer, S.-Y. Lin and M. Luskin, Minimum energy configurations for liquid crystals: computational results, in: Theory and Applications of Liquid Crystals, IMA Vol. Math. Appl., **5**, J. L. Ericksen and D. Kinderlehrer eds., Springer-Verlag, Berlin, 1987, 99-121.

[4] P. G. de Gennes, An analogy between superconductors and smectics A, Solid State Comm., **10** (1972), 753-756.

[5] P. G. de Gennes and J. Prost, The Physics of Liquid Crystals, second edition, Oxford Science Publications, Oxford, 1993.

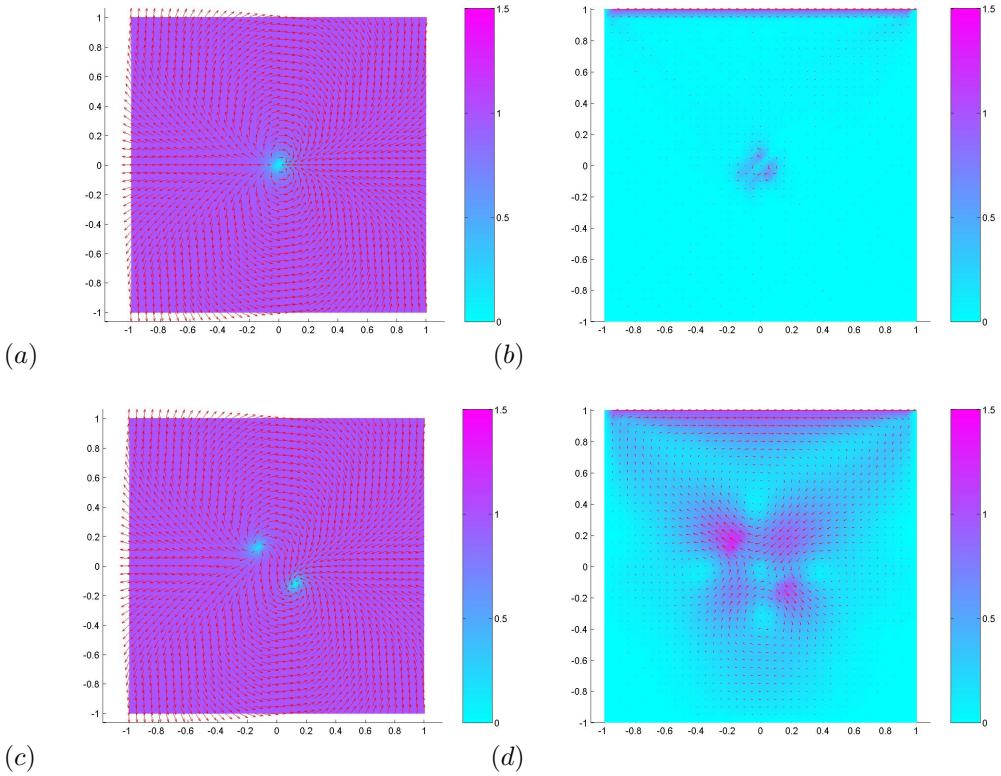

FIGURE 9. Example 4.3: (a) Director field at $t = \Delta t$. (b) Velocity field at $t = \Delta t$. (c) Director field at $t = 0.05$. (d) Velocity field at $t = 0.05$

[6] Q. Du, B. Y. Guo and J. Shen, Fourier spectral approximation to a dissipative system modeling the flow of liquid crystals, SIAM J. Numer. Anal., **39** (2001), 735-762.

[7] R. Glowinski, Finite element methods for incompressible viscous flow. In: Handbook of Numerical Analysis, Vol. IX, P.G. Ciarlet and J.L. Lions, eds, North Holland, Amsterdam, 2003, 31-176.

[8] R. Glowinski, E.J. Dean, G. Guidoboni, L.H. Juarez and T.-W. Pan, Application of operator-splitting methods to the direct numerical simulation of particulate and free-surface flows and to the numerical solution of the two- dimensional elliptic Monge-Ampre equation, Japan J. Ind. Appl. Maths., 25(1), (2008), 1-63.

[9] R. Glowinski, P. Lin and X. B. Pan, An operator-splitting method for a liquid crystal model, Comput. Physics Comm., **152** (2003), 242-252.

[10] R. Glowinski and P. Le Tallec, Augmented Lagrangian and Operator-Splitting Methods in Nonlinear Mechanics, SIAM Studies in Applied Mathematics, **9**, SIAM, Philadelphia, PA, 1989.

[11] R. Hardt and D. Kinderlehrer, Mathematical questions of liquid crystal theory, in: Theory and Applications of Liquid Crystals, J. L. Ericksen and D. Kinderlehrer eds., IMA Vol. Math. Appl., **5**, Springer-Verlag, 1987, 151-184.

[12] F. H. Lin, Nonlinear theory of defects in nematic liquid crystals, phase transitions and flow phenomena, Comm. Pure Appl. Math., **42** (1989), 789-814.

[13] F. H. Lin and C. Liu, Nonparabolic dissipative systems, modeling the flow of liquid crystals, Comm. Pure Appl. Math., **48** (1995), 501-537.

[14] P. Lin, A sequential regularization method for time-dependent incompressible Navier-Stokes equations, SIAM J. Numer. Anal., **34** (1997), 1051-1071.

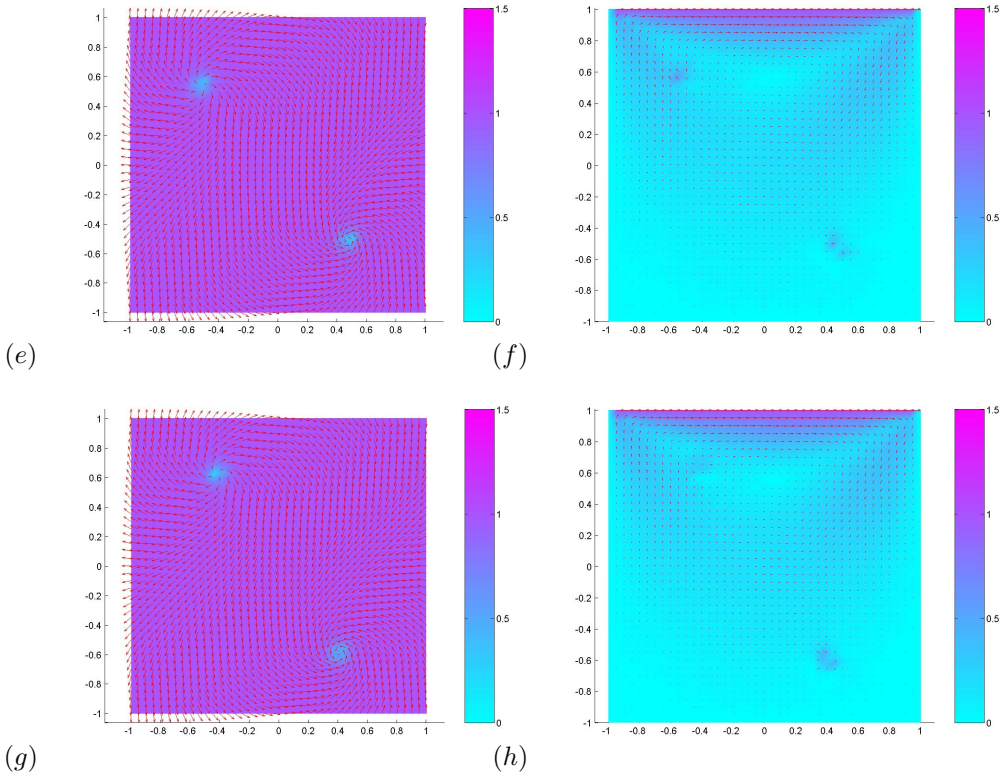

FIGURE 10. Example 4.3: (e) Director field at $t = 1$. (f) Velocity field at $t = 1$. (g) Director field at $t = 3$. (h) Velocity field at $t = 3$

[15] P. Lin, X. Q. Chen and M. T. Ong, Finite element methods based on a new formulation for the non-stationary incompressible Navier-Stokes equations, Int. J. Numer. Meth. Fluids., **46** (2004), 1169-1180.

[16] P. Lin and C. Liu, Simulations of singularity dynamics in liquid crystal flows: A C^0 finite element approach, J. Comp. Phys., **215** (2006), 348-362.

[17] P. Lin and T. Richter, An adaptive homotopy multi-grid method for molecule orientations of high dimensional liquid crystals, J. Comp. Phys., **225** (2007), 2069-2082.

[18] C. Liu and N. J. Walkington, Approximation of liquid crystal flows, SIAM J. Numer. Anal., **37** (2000), 725-741.

[19] C. Liu and N. J. Walkington, Mixed methods for the approximation of liquid crystal flows, M2AN, **36** (2002), 205-222.

[20] W. L. McMillan, Measurement of smectic-A-phase order-parameter fluctuations in the nematic phase of $p-n-$octyloxybenzylidene-p'-toluidine, Physica Review A, **7** (1973), 1673-1678.

Department of Mathematics, University of Houston, Houston, Texas 77204-3476, USA
E-mail: roland@math.uh.edu

Department of Mathematics, University of Dundee, Dundee DD1 4HN, Scotland, UK
E-mail: plin@maths.dundee.ac.uk

Department of Mathematics, East China Normal University, Shanghai 200062, P. R. China
E-mail: xbpan@math.ecnu.edu.cn

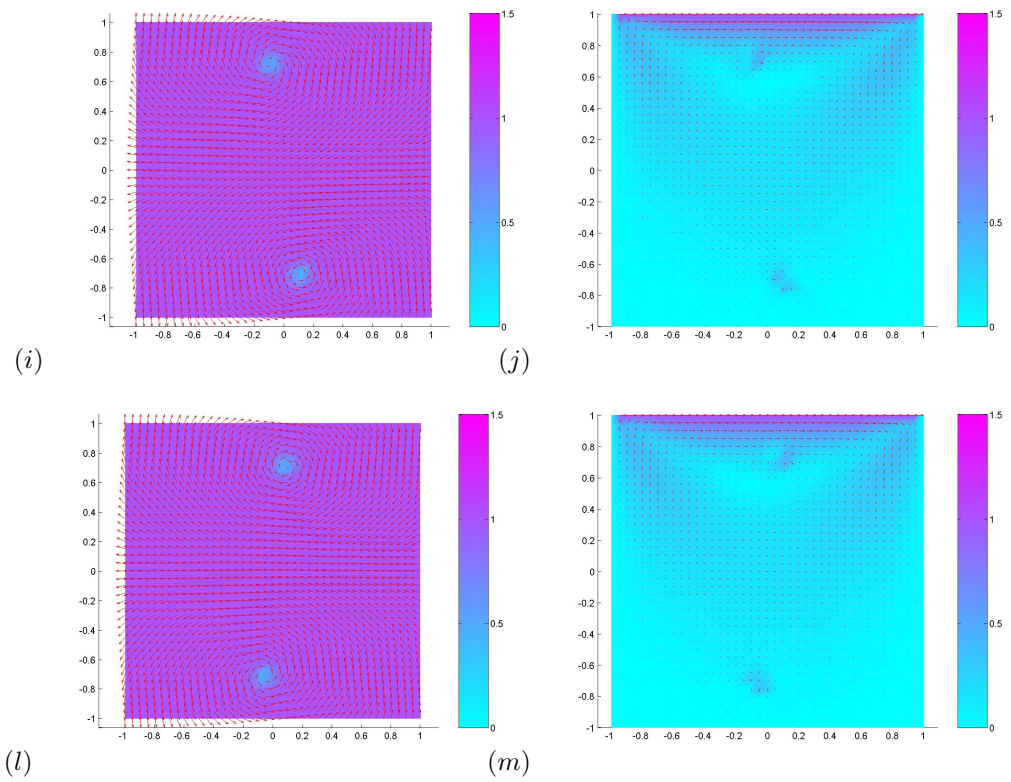

FIGURE 11. Example 4.3: (i) Director field at $t = 10$. (j) Velocity field at $t = 10$. (l) Director field at $t = 20$. (m) Velocity field at $t = 20$